A Frequency-Domain Model for a Novel Wave Energy Converter

Y. Wei*, Z. Yu*, J.J. Barradas-Berglind†, M. van Rooij*, W.A. Prins*, B. Jayawardhana† and A.I. Vakis*

*Advanced Production Engineering, Engineering and Technology Institute Groningen,
Faculty of Science & Engineering, University of Groningen,
Nijenborgh 4, Groningen 9747AG, The Netherlands

†Discrete Technology & Production Automation, Engineering and Technology Institute Groningen,
Faculty of Science & Engineering, University of Groningen,
Nijenborgh 4, Groningen 9747AG, The Netherlands

***Abstract*—In this work, we develop a frequency-domain model for the novel Ocean Grazer (OG) wave energy converter (WEC), with the intention to study the hydrodynamic behavior of its array of floater elements individually connected to power take-off (PTO) systems. To investigate these hydrodynamic interactions, we lean on the boundary element method (BEM) open-source code NEMOH, in order to solve the scattering and radiation problem. The interconnection between the floater elements is realized through hinges, which add extra constraint equations to the multibody problem. In particular, we illustrate this with a floater array consisting of ten hinged floater elements in open sea conditions, which we verify by comparing it with our previously developed time-domain model. Accordingly, the hydrodynamic behavior of the floater array is quantified by the response amplitude operator (RAO) of the floater elements and the extracted energy. The present work will be instrumental in the synthesis of advanced control algorithms for the OG-WEC.**

***Index Terms*—Frequency domain model, Ocean Grazer, multi-body interaction, wave energy converter**

I. Introduction

The recently proposed novel wave energy converter (WEC) that constitutes the core technology of the Ocean Grazer (OG), a hybrid ocean energy collection and storage platform, has the potential to be an effective contender in the challenge of extracting the latent energy from offshore oceanic waves. The OG-WEC utilizes an adaptable multi-pump multi-piston power take-off (MP^2PTO) system that consists of a grid of inter-connected floater elements —termed a floater blanket—, with each floater element being connected to a piston-type hydraulic pumping system —a multi-piston pump (MPP) [1]. Each MPP consists of three differently-sized engageable pistons, which allow for seven different pumping combinations. Our previous work has demonstrated that the adaptable MPP unit, through a simple control algorithm, can extract more energy than constant piston combinations [2]; furthermore, we showed that the overall energy extraction of the MP^2PTO system can be improved by optimising the set of MPPs according to the incident waves. Nevertheless, due to the fact that the possible configurations of MPPs increase dramatically as the number of floater elements increases, it is computationally costly to identify the optimal configurations of the MP^2PTO system via our time-domain-based numerical model.

Hence, to determine the PTO configuration of the MP^2PTO system in the face of a wide variety of sea conditions a number of issues must be tackled. The first one, which is addressed in the present paper, is to develop a frequency-domain model to investigate the hydrodynamics of the floater blanket in a numerically tractable fashion. The dynamics of the floater elements are mainly dominated by two physical phenomena: (I) the interaction between the multibody system and the wave; and, (II) the dynamics of the rigid multibody system. There has been extensive work dealing with these two problems, particularly for wave energy applications, using various numerical model [3], [4] and mathematical models [5], [6].

In general, a wave farm consists of WEC arrays, giving rise to a multibody and wave interaction problem. Therefore, the extracted energy of a WEC in a farm is not only determined by the incident wave, but also by the radiated/diffracted waves from neighboring WECs. The latter may become more relevant as the gaps between the WECs become smaller, which may be utilized to increase the overall extracted energy of the wave farm. For example, the work in [5] compared the wave power extraction of a large buoy with a compact array of small buoys. Results indicate that the latter system with many degrees of freedom had a higher efficiency for a much broader bandwidth. The authors in [6], gave a mathematical solution for a flap gate farm WEC, which consists of multiple bottom-hinged floater bodies pitching under the incident waves, in an infinitely long channel; it was found that employing a larger number of much smaller devices in trapped resonant modes had a beneficial effect on the system performance.

For a single device, there have been several WEC concepts that consist of arrays of jointed hydrodynamic elements, taking advantage of their relative motion to extract energy, e.g., the Hagen-Cockereil WEC [7], the Pelamis WEC [8] and the hinge-barge WEC [3], [4]. To solve the dynamic response of the joint elements, additional constraint equations need to be introduced. In [9], an approximate analysis of a flexible or

hinged raft was provided, which could be applied to estimate the performance of any elongated floating vessel. In [10], a hydrodynamic model to investigate the wave extraction by a train of rafts was proposed. Subsequently, in [7], the previous approach was employed to investigate the performance of a parallel array of rectangular pontoons in a channel. The Pelamis WEC, which was the first offshore device to provide electricity to the grid in 2004, consists of a series of semi-submerged cylindrical sections linked by hinged joints. This concept has been extensively modeled using various numerical techniques [8], but unfortunately there are few open reports available. Recently, researchers proposed a joint-coordinate approach in the time-domain, aiming to represent the fully non-linear joints of the hinge-barge WEC [4]; this approach was applied to study a 3-hinged-barge system.

Although the floater blanket of the OG is conceptually similar to the WEC arrays of a wave farm, or single WECs with jointed floating components, it has some unique features. It is different from the WEC array, since for such arrangements there are no physical connections between the WECs and, in addition, the gaps between the WECs are generally large (with respect to their dimensions). It is also different from the multi-element single WECs, whose elements are significantly fewer in comparison. Moreover, the floater blanket is projected to be mounted on the massive OG platform through hundreds of cables. Thus, the coupling dynamics of the floater blanket and platform may affect the overall performance of the device, which requires careful investigation.

The main contribution of this paper is to perform the preliminary investigation of the hydrodynamic behavior of a one-column floater array with hinged elements in the open sea. The array is perpendicular to the wave front of the incident wave like a line absorber. The hydrodynamic coefficients are calculated by means of the open-source code NEMOH, which enables us to solve the scattering and radiation problems for an array of floating bodies. The dynamics of the floater elements are handled by solving a set of motion equations of the multibody system and additional constraint equations introduced by the coupling with hinges. We illustrate our findings through a series of simulations, where we calculate the response amplitude operator (RAO) of the floater elements and the extracted energy of the PTOs.

The remainder of the paper is organized as follows: the numerical model is described in Section II. Consequently, the frequency-domain model is verified in Section III-A by comparing it against our time-domain model. Based on the former model, the effects of body-to-body (B-B) interaction and constrains on the floater element dynamics are investigated in Section III-B. Lastly, conclusions and further research directions are given in Section IV.

II. NUMERICAL MODEL

In the OG concept, a floater blanket consists of hundreds of interconnected floater elements and it is mounted on a massive platform, which introduces a great number of degrees of freedoms (DOFs) into the system. Unfortunately, there is not yet any existing mature device that can guide the design of the current complex system. Hence, we decide to firstly perform the preliminary investigation on a one-column floater array comprised of simple box-shape floaters, aiming to establish the basic understanding on the hydrodynamics of continuous floating bodies in waves. This simple numerical benchmark may be directly compared with experimental results in the future. The aim of the previous is to lay the foundations of a comprehensive model of a multi-column floater blanket coupled to the OG platform. In the present model, it is assumed that: the fluid is an irrotational, inviscid, incompressible ideal fluid and that potential theory is applicable; the wave amplitude is small so that it satisfies linear wave theory; the body motion is small such that small-angle approximations can be adopted.

A. Motion and Constraint equations

Consider the motion equations for a floater array comprised of M elements, where we used the index m to describe the m^{th} floater element, such that

$$\boldsymbol{M}^{(m)}\ddot{\boldsymbol{X}}^{(m)} = \boldsymbol{F}_e^{(m)} + \boldsymbol{F}_r^{(m)} + \boldsymbol{F}_{hs}^{(m)} + \boldsymbol{F}_h^{(m)} + \boldsymbol{F}_{pto}^{(m)}, \quad (1)$$

where $\boldsymbol{M}^{(m)} \in \mathbb{R}^{6\times6}$ is a diagonal matrix of masses and moments of inertia for the general case of a floater with 6 DOFs. We denote $\boldsymbol{X}^{(m)} = [x_1^{(m)}, \ldots, x_6^{(m)}]^\top$ as the displacement vector of the m^{th} floater, whose elements represent the surge, sway, heave, roll, pitch and yaw displacements, respectively. Furthermore, $\boldsymbol{F}_e^{(m)} \in \mathbb{R}^6$ is the wave excitation force vector; $\boldsymbol{F}_r^{(m)} \in \mathbb{R}^6$ is the radiation force vector composed of the radiation forces due to the motion of the floater m itself as well as other floater elements; $\boldsymbol{F}_{hs}^{(m)} \in \mathbb{R}^6$ is the restoring force vector, which arises when the floater is perturbed away from its equilibrium; $\boldsymbol{F}_h^{(m)} \in \mathbb{R}^6$ is the overall internal force vector due to the hinges at both ends of the floater; and $\boldsymbol{F}_{pto}^{(m)} \in \mathbb{R}^6$ is the PTO force vector.

The radiation force $\boldsymbol{F}_r^{(m)}$ includes added-mass and wave damping terms, which can be written as

$$\boldsymbol{F}_r^{(m)} = -\sum_{n=1}^{M}\left(\boldsymbol{A}^{(m,n)}\ddot{\boldsymbol{X}}^{(n)} + \boldsymbol{C}^{(m,n)}\dot{\boldsymbol{X}}^{(n)}\right) \quad (2)$$

where $\boldsymbol{A}^{(m,n)}, \boldsymbol{C}^{(m,n)} \in \mathbb{R}^{6\times6}$ are the frequency-dependent added-mass and damping coefficient matrices, respectively. Note that the superscripts m and n denote the radiation force of floater m as a result of the motion of floater n.

In addition, $\boldsymbol{F}_{hs}^{(m)}$ is a linear function of the heave, pitch and roll perturbations, which is expressed in terms of motions about the centre of gravity as

$$\boldsymbol{F}_{hs}^{(m)} = -\boldsymbol{K}_{hs}^{(m)}\boldsymbol{X}^{(m)} \quad (3)$$

where $\boldsymbol{K}_{hs} \in \mathbb{R}^{6\times6}$ corresponds to the hydrostatic stiffness matrix that specifies the variation of the net weight and buoyancy load with respect to the changes in position from equilibrium [11].

A sketch showing the convention of the displacements and forces on the floaters is shown in Fig. 1. The dashed-line

floaters represent their original position on the still water surface. The local coordinate of each floater is located at its centre of gravity. We number the right and left hinges of

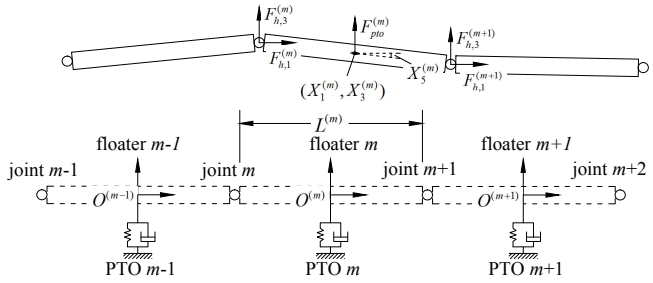

Fig. 1. Sketch of the displacements and forces on floater m.

the m^{th} floater as hinge m and hinge $m+1$, respectively. Consequently, the composition of the hinge forces at both ends $\boldsymbol{F}_h^{(m)}$ can be conveniently expressed in matrix form as

$$\boldsymbol{F}_h^{(m)} = \begin{bmatrix} F_{h,1}^{(m)} - F_{h,1}^{(m+1)} \\ 0 \\ F_{h,3}^{(m)} - F_{h,3}^{(m+1)} \\ 0 \\ \frac{F_{h,3}^{(m)} L^{(m)}}{2} + \frac{F_{h,3}^{(m+1)} L^{(m)}}{2} \\ 0 \end{bmatrix} \tag{4}$$

where $F_{h,1}, F_{h,3} \in \mathbb{R}$ are the constraint forces in the surge and heave directions at the hinge joints respectively; $L^{(m)} \in \mathbb{R}$ is the length of floater m.

A simple PTO is considered in the present paper, whose mechanism is represented as a linear spring-damper system. Since the floater extracts energy from the wave heave, we assume that the PTO force in the heave direction is linearly proportional to the heave motion of the floaters, namely

$$F_{pto,3}^{(m)} = -K_{pto}^{(m)} x_3^{(m)} - C_{pto}^{(m)} \dot{x}_3^{(m)} \tag{5}$$

where $F_{pto,3}^{(m)}$ is the third entry of $\boldsymbol{F}_{pto}^{(m)}$, corresponding to heave motion; K_{pto} is the stiffness of the PTO and C_{pto} is the damping of the PTO. Consequently, we consider all other elements of $\boldsymbol{F}_{pto}^{(m)}$ to be zero. We acknowledge that the PTO forces in the MP^{2}PTO system are highly non-linear and cannot be explicitly described by a linear PTO. This non-linearity stems from the engaging and disengaging of piston combinations, which allows the OG-WEC to adapt to different sea states; details of the MP^{2}PTO system can be found in [1]. The inclusion of a non-linear PTO force in a frequency domain model is not straightforward [12]. A higher order model could be developed in order to deal with the pumping force in the future.

Substituting the force vectors in (2)-(5) into (1) and assuming that the forces and motions are harmonic with a frequency ω, we obtain the motion equation in terms of complex amplitudes, which is

$$\begin{aligned} &\Big[-\omega^2 \left(\boldsymbol{M}^{(m)} + \boldsymbol{A}^{(m,m)} \right) + i\omega \left(\boldsymbol{C}^{(m,m)} + \boldsymbol{C}_{pto}^{(m)} \right) \\ &\qquad + \left(\boldsymbol{K}_{hs}^{(m)} + \boldsymbol{K}_{pto}^{(m)} \right) \Big] \hat{\boldsymbol{\xi}}^{(m)} \\ &+ \sum_{n=1, n\neq m}^{M} \left(-\omega^2 \boldsymbol{A}^{(m,n)} + i\omega \boldsymbol{C}^{(m,n)} \right) \hat{\boldsymbol{\xi}}^{(n)} - \hat{\boldsymbol{F}}_h^{(m)} = \hat{\boldsymbol{F}}_e^{(m)} \end{aligned} \tag{6}$$

where $\hat{\boldsymbol{F}}_e$, $\hat{\boldsymbol{F}}_h$ and $\hat{\boldsymbol{\xi}} \in \mathbb{C}^6$ are the complex amplitude vectors of the excitation force, hinge force and floater displacement, respectively; $\boldsymbol{F}_e = \Re\left\{\hat{\boldsymbol{F}}_e e^{i\omega t}\right\}$, $\boldsymbol{F}_h = \Re\left\{\hat{\boldsymbol{F}}_h e^{i\omega t}\right\}$ and $\boldsymbol{X} = \Re\left\{\hat{\boldsymbol{\xi}} e^{i\omega t}\right\}$ represent their real part. On the left-hand side of (6), the first term includes the general free floating element forces with PTO, the second term represents the B-B radiation, and the third term incorporates the hinge constrains.

It is assumed that the amplitudes of the floater displacements are small and the floater elements are considered as rigid bodies. The displacements at the hinges (see Fig. 1) must satisfy

$$\begin{aligned} \hat{\xi}_1^{(m)} &= \hat{\xi}_1^{(m+1)} \quad \text{and} \\ \hat{\xi}_3^{(m)} - \frac{L^{(m)}}{2} \hat{\xi}_5^{(m)} &= \hat{\xi}_3^{(m+1)} + \frac{L^{(m+1)}}{2} \hat{\xi}_5^{(m+1)}, \end{aligned} \tag{7}$$

which constrain the motion in the surge and heave directions.

At the end of the floater column, we suppose that there is a zero-mass virtual floater following floater M, which only has translational motion with respect to the virtual hinge $M+1$. Hence, (6)-(7) constitute $8M+2$ simultaneous algebraic equations for unknowns $\hat{\boldsymbol{\xi}}$ and $\hat{\boldsymbol{F}}_h$. In order to solve the system of equations, additional constraint equations have to be imposed at the hinges 1 and $M+1$. Therefore, the forces at the virtual hinge $M+1$ are zero, and the pitch motion of the virtual floater $M+1$ is zero, such that

$$\hat{\xi}_5^{(M+1)} = 0, \quad \hat{F}_{h,1}^{(M+1)} = 0 \quad \text{and} \quad \hat{F}_{h,3}^{(M+1)} = 0 \tag{8}$$

Analogously, for hinge 1, depending on the types of its constraints, additional equations may be required. Two different scenarios are investigated in the present paper: (A) when the floater array is anchored to the sea bottom and the surge motion of the floater 1 is zero; (B) when the floater array is freely floating on the water surface, making the hinge forces at hinge 1 equal to zero. Scenario (A) can be formulated as

$$\hat{\xi}_1^{(1)} = 0 \quad \text{and} \quad \hat{F}_{h,3}^{(1)} = 0, \tag{9}$$

whereas scenario (B) can be described by

$$\hat{F}_{h,1}^{(1)} = 0 \quad \text{and} \quad \hat{F}_{h,3}^{(1)} = 0. \tag{10}$$

After imposing the above constraint equations to the assembled system, a solution can be obtained.

The performance of the WEC can be evaluated by the captured energy. According to [13], the time-averaged capture power of each PTO can be calculated with the heave

displacement as

$$\bar{P}^{(m)} = \frac{1}{2} C_{pto}^{(m)} \omega^2 |\hat{\xi}_3^{(m)}|^2, \tag{11}$$

such that the overall capture power is obtained by summing up the power of the individual PTOs, namely

$$\bar{P}_s = \sum_{m=1}^{M} \bar{P}^{(m)}. \tag{12}$$

B. Model parameters and Considerations

In the present paper, a floater array comprised of ten floater elements is investigated. The relevant parameters of the model are summarized in Table I. The geometry of the floater is simplified as that of a rectangular cuboid; additionally, the floater is considered as a lightweight body, which will be assembled by foam-like elements in our initial design. Hence, the mass of the floater used here is much smaller than other floating WECs. We assume that half of the floater is initially submerged in the water. According to the numerical study on the Pelamis WECs [14], varying the draft of the device does not have much influence on energy extraction; we do not investigate the draft effects in the present paper. It is worth noting that, since the operating principle of the OG-WEC is to pump working fluid from a lower to an upper reservoir, heavy static loads may be exerted on the floaters due to the significantly large water head between the aforementioned reservoirs. Each floater can vary its PTO setting to respond to the incident waves. Theoretically, there are optimal PTO configurations in the floater blanket which can maximize the energy extraction under the incident wave with specific frequency. Nevertheless, determining such PTO configurations is challenging and would require to solve an optimization problem, which is out of the scope of this paper. Hence we use constant stiffness and damping coefficients for all PTOs. The OG-WEC is suggested to be operated offshore with abundant wave energy resources. The water depth of 600 m is used in the simulation.

TABLE I
PARAMETERS OF THE NUMERICAL MODEL

Description	**Value**
Number of floaters	10
Dimension of floater ($L \times W \times H$) [m]	$7 \times 7 \times 2$
Volume of floater [m^3]	98
Mass of floater [kg]	1500
Draft [m]	1
Stiffness of PTO [N/m]	5.8×10^4
Damping of PTO [N/(m.s)]	1.1×10^4
Water depth [m]	600
Density of water [kg/m^3]	1025

Due to the symmetry of the problem, only half of the geometry surface is meshed in NEMOH. The mesh convergence study indicates that convergence is achieved when there are 26 panels on each floater (about 1.6 m^2 per panel). In the following study, we use this mesh for the simulation. As we aim to develop the OG-WEC to efficiently extract energy for a wide range of wave periods, the hydrodynamic responses of the WEC to waves with periods between 4 s and 20 s are considered here.

III. Results and Discussion

A. Comparison with the time domain model

In order to verify the proposed numerical model, the results of the frequency-domain (FD) model are compared against the results produced by our recently developed time-domain (TD) model [2], which is based on the open-source WEC-Sim code [15], a block diagram model developed based on Simulink® and Simscape Multibody™. The hydrodynamic coefficients required for the model —$\boldsymbol{A}$, $\boldsymbol{B}$ and $\hat{\boldsymbol{F}}_e$— can be numerically obtained from universal BEM solvers, e.g., WAMIT, AQWA and NEMOH. In the present paper, we lean on the potential flow BEM-based open-source solver NEMOH [16] to calculate these coefficients. The sketch of the TD model schematic is shown in Fig. 3.

The floaters are physically joined by the hinges, which only allow relative rotation between their neighbours. Each floater is connected to a linear PTO. The floater blanket will be anchored to the seabottom or platform. Therefore, a pin slot joint is applied to the first floater to restrict its surge motion. Both models are calculated with the same outcomes from NEMOH. The applied damping of PTOs can been seen in Table I. Fig. 2 depicts the comparison of the response amplitude operators (RAOs) in heave of the floaters between the two models, and excellent agreement is demonstrated. Good agreement is also obtained from the comparison of the RAOs in other DOFs, which are not presented here.

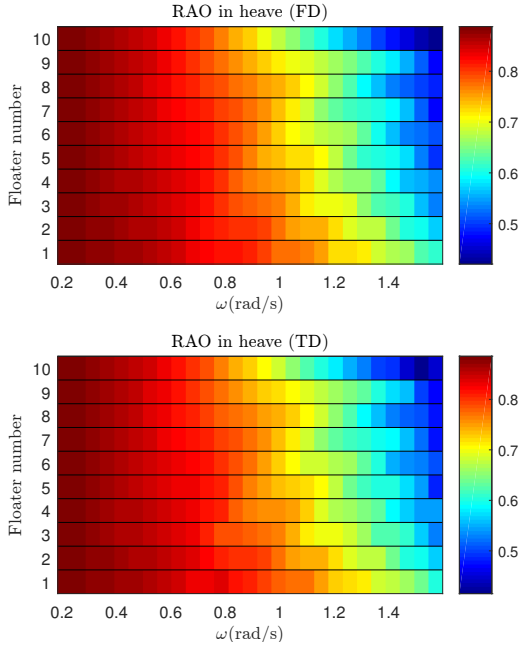

Fig. 2. Comparison of RAOs in heave between the FD model and TD model.

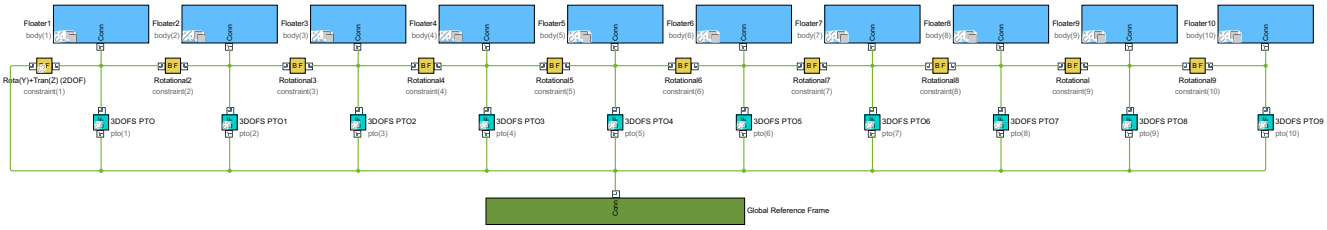

Fig. 3. TD model of the floater array with linear PTOs. The blue blocks represent the floater elements; they are hinged with the revolute joints (the yellow block); each floater element is connected to an individual linear PTO (the cyan block); all the PTOs are mounted to the seabottom (the dark green block).

Due to the lightweight design of the floaters, they have relatively small inertia but large hydrostatic stiffness. The motion of the floaters may be sensitive to the force components given in (1). The resonance frequency is small and out of our range of interest. Thus, the RAOs in heave are always less than 1 and decrease with the wave frequency. When encountering a low frequency wave, the floaters move synchronously with the wave evolution, such that their RAOs are almost the same. As the wave frequency increases, the excitation forces in heave decrease because the incident waves are diffracted away from the floater array, resulting in the decrease of the heaving responses. The RAOs also show a general decreasing trend from the first floater to the last for high frequency waves, although there are slight fluctuations between adjacent floaters. The reason for this is that the diffraction and radiation effects become significant when the length of the floater array is comparable to the wavelength. The superposition of the diffracted/radiated waves with the incident wave may amplify the wave at some specific positions; this will be further discussed in Section III-B.

Thanks to the excellent agreement of the RAOs between the two models, the capture power of each floater matches very well for the two models, although there are slight discrepancies in a few floaters for high frequency waves, as it can be observed in Fig. 4. The power capture of the floaters for low frequency waves is generally lower than for high frequency waves but does not increase monotonically. For example, the capture power at floater 5 has two local peaks at $\omega \approx 1.2$ rad/s and $\omega \approx 1.4$ rad/s, which are associated with the complex wave field mentioned previously.

The overall capture power of the floater array from the two models is shown in Fig. 5. The captured power of the TD model is slightly lower than that of the FD model for high frequency waves, but the match is perfect for low frequency waves. Thus, we can conclude that the proposed FD model is accurate enough to investigate the hydrodynamics of the floater array and the overall performance of the device. The computational time of the FD model is negligible compared to that of the TD model. Hence, due to its computational efficiency, the present FD model is suitable to search for the optimum PTO configurations of the OG-WEC.

From Fig. 5, we can see that the maximum energy extraction is achieved at $\omega \approx 1.4$ rad/s. The simulations with various PTO settings were also carried out. It was found that varying both the stiffness and damping coefficients of the PTOs merely

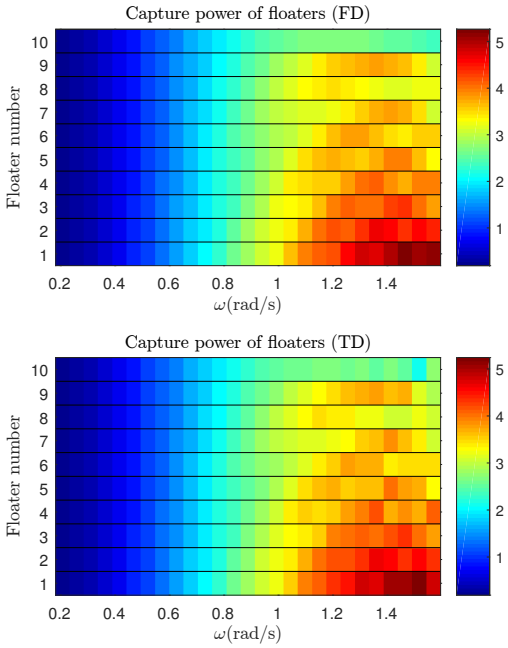

Fig. 4. Comparison of capture powers of floaters (unit: kW) between the FD model and the TD model.

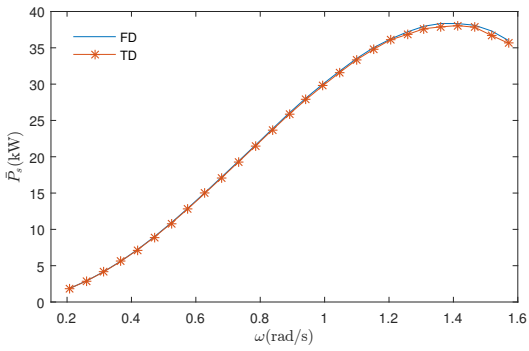

Fig. 5. Comparison of overall capture power (unit: kW) between FD model and TD model.

changes the magnitude of the power, but does not alter the frequency where the maximum energy extraction is obtained. An exception to this is when an extremely large damping coefficient is applied, which results in that frequency being shifted to a lower one.

B. Case studies

The floater blanket is a novel concept to extract wave energy, whose hydrodynamic behavior has not yet been investigated. The motion of the elements in the floater blanket is driven by the hydrodynamic forces and restricted by hinges. In order to understand such behaviors, we investigate —through a series of case studies—the contribution of the hydrodynamic and constraint forces on the floater response, based on the motion equations described in Section II.

Three different types of scenarios are proposed for the investigation, resulting in eight possible combinations, which are listed in Table II and sketched in Fig. 6. The results of *case*1–6 will be discussed in the paper; *cases*7&8 which omit B-B radiation are not considered in the paper because B-B radiation effects are inevitable in reality.

TABLE II
CONFIGURATIONS FOR CASE STUDIES

Cases	B-B radiation	Hinge constraint	Surge constraint
*case*1	✓	✓	✓
*case*2	✗	✓	✓
*case*3	✓	✗	✓
*case*4	✓	✓	✗
*case*5	✗	✗	✓
*case*6	✓	✗	✗
*case*7	✗	✓	✗
*case*8	✗	✗	✗

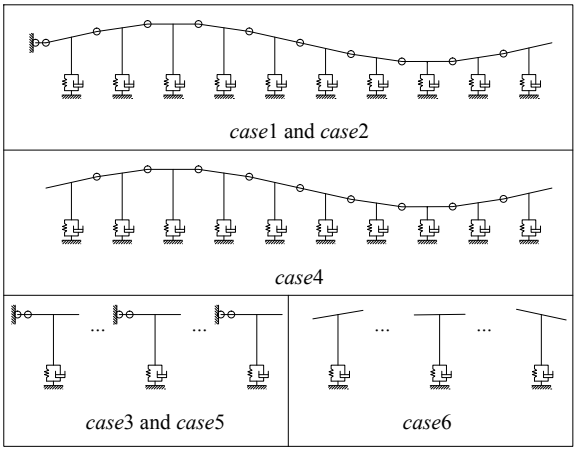

Fig. 6. Sketch of constraints used in different scenarios.

The scenarios in Table II exemplify situations that are relevant in answering the following questions of concern:

- How important is the role of the B-B radiation on the system dynamics and energy extraction?
- Is the idea of using jointed (hinged) floater elements to form a floater array beneficial for capturing wave energy?
- Can the additional constraints on the floater array improve the performance of the device?

Based on these scenarios, the six cases are conducted in the present work, which are briefly described as follows:

- *case*1 is a general case where the floater array is anchored to the seabottom and responds to the incident wave;
- *case*2 neglects the B-B radiation, i.e., by omitting the second term at the left-hand side of (6);
- *case*3 removes the hinges between the floater elements, but restricts their surge motion individually (each floater has independent heave and pitch motions);
- *case*4 allows the floater array to be free floating in waves, and the floater elements have consistent surge motion, i.e., (10) is applied to the system;
- *case*5 is similar to *case*3, but does not account for the B-B radiation. The floater elements are considered as independent heave absorbers.
- *case*6 completely releases the constraints on the floater elements. All elements have six DOFs.

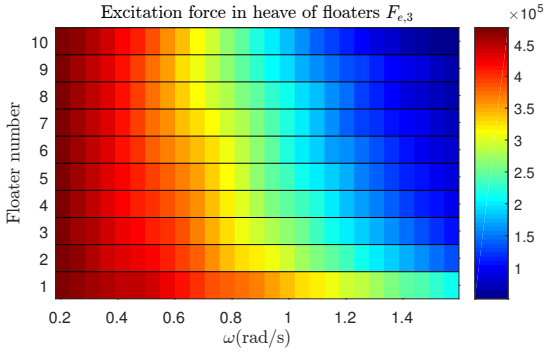

Fig. 7. Excitation force coefficients in heave of floaters (unit: N) computed with NEMOH.

The excitation force coefficients in the heave direction of floaters corresponding to the six aforementioned cases are depicted in Fig. 7. One can see that the forces for low frequencies are almost equal. It is well known that low frequency waves have minimal diffraction. The presence of the floater array does not sufficiently disturb the pressure field due to the incident waves and the excitation force is mainly attributed to the Froude-Krylov force, which is the same for all floater elements. As the wave frequency increases, the excitation force on each floater decreases because of the relative importance of diffraction effects under high frequency waves. The force acting on the first floater is the maximum of the ten floaters due to the fact that the incident waves are mainly diffracted by the first floater, resulting in declining wave amplitudes at the location of the following ones. However, the wave energy may be partly compensated by the diffracted waves at some specific floaters, such that a slight variation can be observed in the last few.

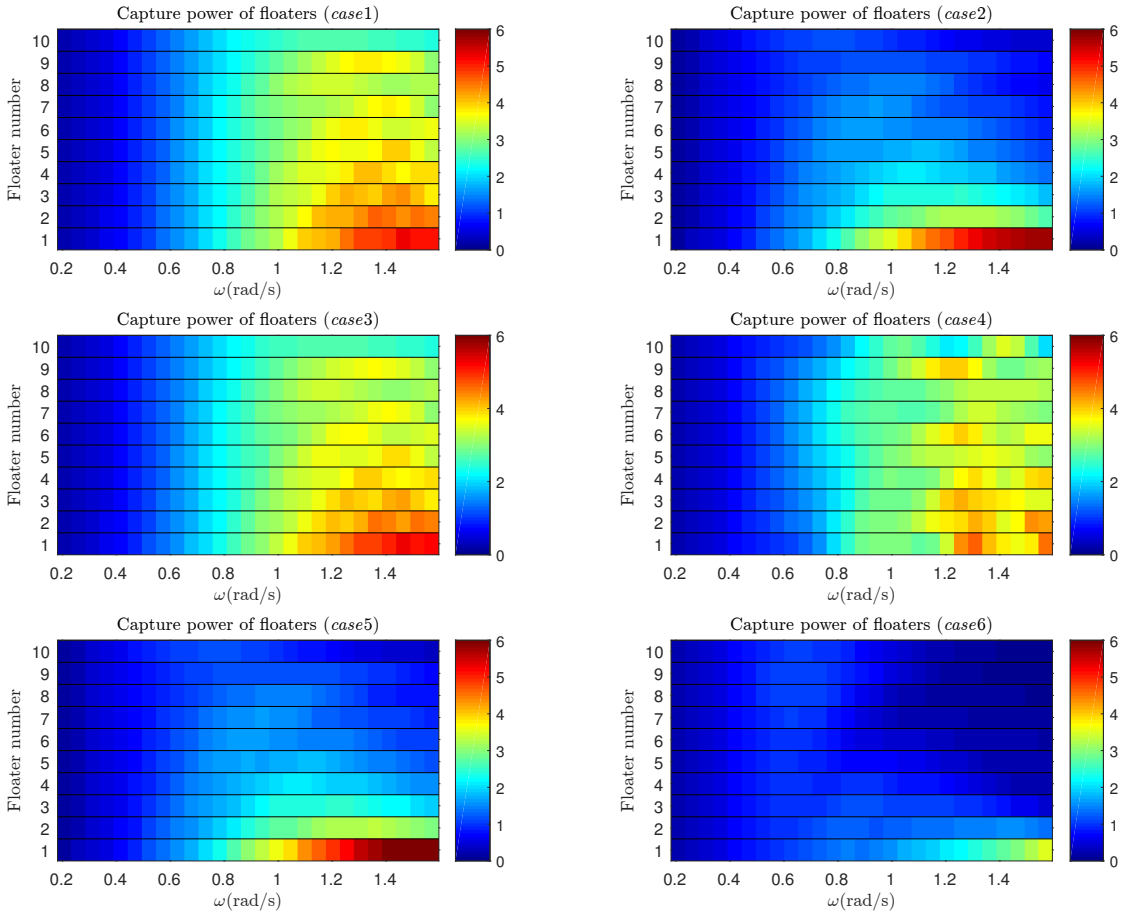

Fig. 8. Capture power of floaters (unit: kW) in various scenarios.

The captured power of the floaters of the six cases is presented in Fig. 8, which gives an intuitive impression of the performance of each element with wave frequency in various scenarios. Based on the results of Fig. 8, one can calculate

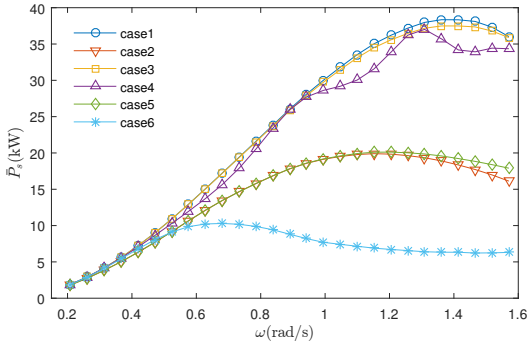

Fig. 9. Overall capture power (unit: kW) of the floater array for various scenarios.

the overall capture power of the whole floater array, which is shown in Fig. 9. It can be observed that *case*1 outperforms the other five cases; *case*3 and *case*4 can extract slightly less energy than *case*1; *case*2 and *case*5 show similar trends with wave frequency, and there is great reduction for both scenarios compared to *case*1; lastly, *case*6 is the worst scenario, which can only capture about 15% of the energy of *case*1 for high frequency waves.

Both *case*2 and *case*5 omit the B-B radiation terms in (6). Hence, the capture power of floater 1 for both cases is significantly greater than for other floaters. While comparing with *case*1, it is observed that the capture power of the floaters in both cases is generally smaller than that of *case*1, except for floater 1. This is because the B-B radiation terms essentially represent the energy-redistribution process due to the motion of the floaters. The superposition of the radiated and diffracted waves may strengthen or cancel the waves at the locations of the floaters, resulting in an increase or decrease of energy extraction on those floaters. In terms of overall capture power, the B-B radiation becomes more important as wave frequency increases. Neglecting such effects may underestimate the capture power by over 50%. It indicates that the radiated energy by one floater element in an array may be captured by adjacent floaters, which reduces the net radiation loss of the system and improves the overall performance of the device.

The main difference between *case*1 and *case*3 is that *case*3 allows free pitch motion. It seems that the free pitch motion

does not significantly influence the system dynamics. The hydrodynamic behavior between these two cases is very close, and the overall power of *case*3 is only slightly smaller than that of *case*1. Similar results can be observed for *case*2 and *case*5, where there is only a small difference in overall capture power between them for high frequency waves. Therefore, it is concluded that the free pitch motion of the floater elements is likely irrelevant to the floater hydrodynamics and the device performance.

On the other hand, the whole floater array in *case*4 has free surge motion in contrast to *case*1; the reduction of its overall capture energy with that of *case*1 is more considerable. The extracted energy of each floater demonstrates different characteristics. It appears that the system tends to balance the capture power of the elements in the floater array in *case*4, as the difference between the floater 1 and other floaters is reduced. The worst scenario (*case*6) allows free pitch and surge motions. It is found that the variation of pitch is insignificant while that of surge is considerably amplified, compared to *case*1. Thus, the great reduction of power in *case*6 should be mainly attributed to the allowance of the surge motion. The variation of the free surge motion can also be mathematically explained with the motion equation of surge. Increasing the mass in motion equation of surge can reduce its RAO in surge. The mass of the floater in *case*6 is 1500 kg, and the motion equations of the ten floaters in surge mode can be combined into one in *case*4 with a mass of 10×1500 kg because ten hinged floaters will surge together, while that mass in *case*1 is essentially infinite since its surge motion is fully restricted to be zero. Hence, *case*6 exhibits maximum surge motion.

It was commonly thought that reducing the DOFs might be disadvantageous to the device performance. Our current findings are in agreement with this statement. Based on the above discussion, restricting the surge motion of the floaters is more crucial than pitch motion to increase power capture. Therefore, joining the floater elements of the floater array with hinges is not critical to the device performance; however, the reduction of the surge motion of the floater elements is beneficial for the energy extraction.

IV. Conclusions

This paper develops a frequency-domain numerical model of the one column floater array consisting of ten hinged elements. Accordingly, we investigate its hydrodynamic behavior described by this model in the open sea. Based on the numerical results, we can draw the following conclusions:

- Good agreement is obtained between the TD model and the FD model. The FD model is superior for its high computational efficiency.
- The body-to-body interaction via radiation has to be accounted for; omitting such effects might underestimate the capture power by over 50%.
- The hinge constraints change little the performance of the device, while restricting the surge motion of the floater array can significantly increase the energy extraction.

This work only investigated the hydrodynamics of a ten-element floater array in the open sea. Further work will focus on the multi-column and -row element floater blanket and its coupling with the platform. In addition, the PTOs in the present study are purely linear, which is completely different from our MP^{2}PTO system. Accounting for the nonlinearity of the pumping force —due to the engaging and disengaging of pistons— together with the frequency domain model may be a challenging subject that merits further investigation.

References

[1] A. Vakis and J. S. Anagnostopoulos, "Mechanical design and modeling of a single-piston pump for the novel power take-off system of a wave energy converter," *Renewable Energy*, vol. 96, Part A, pp. 531 – 547, 2016. [Online]. Available: http://www.sciencedirect.com/science/article/pii/S0960148116303780

[2] Y. Wei, J. Barradas-Berglind, M. van Rooij, W. Prins, B. Jayawardhana, and A. Vakis, "Investigating the adaptability of the multi-pump multi-piston power take-off system for a novel wave energy converter," *Renewable Energy*, vol. 111, pp. 598 – 610, 2017. [Online]. Available: http://www.sciencedirect.com/science/article/pii/S096014811730349X

[3] G. Nolan, M. Ó Catháin, J. Murtagh, and J. Ringwood, "Modelling and simulation of the power take-off system for a hinge-barge wave-energy converter," 2003.

[4] D. Padeletti, R. Costello, and J. V. Ringwood, "A multi-body algorithm for wave energy converters employing nonlinear joint representation," in *ASME 2014 33^{rd} International Conference on Ocean, Offshore and Arctic Engineering*. American Society of Mechanical Engineers, 2014.

[5] X. Garnaud and C. Mei, "Comparison of wave power extraction by a compact array of small buoys and by a large buoy," *IET Renewable Power Generation*, vol. 4, no. 6, pp. 519–530, 2010.

[6] P. Sammarco, S. Michele, and M. dErrico, "Flap gate farm: From Venice lagoon defense to resonating wave energy production. Part 1: Natural modes," *Applied Ocean Research*, vol. 43, pp. 206–213, 2013.

[7] P. Haren and C. C. Mei, "An array of Hagen-Cockerell wave power absorbers in head seas," *Applied Ocean Research*, vol. 4, no. 1, pp. 51 – 56, 1982. [Online]. Available: http://www.sciencedirect.com/science/article/pii/S0141118782800217

[8] R. Yemm, R. Henderson, and C. Taylor, "The OPD Pelamis WEC: Current status and onward programme," in *Proceedings of 4^{th} European Wave Energy Conference*, Alborg, Denmark, 2000.

[9] J. Newman, "Absorption of wave energy by elongated bodies," *Applied Ocean Research*, vol. 1, no. 4, pp. 189 – 196, 1979. [Online]. Available: http://www.sciencedirect.com/science/article/pii/0141118779900269

[10] P. Haren and C. C. Mei, "Wave power extraction by a train of rafts: Hydrodynamic theory and optimum design," *Applied Ocean Research*, vol. 1, no. 3, pp. 147–157, 1979.

[11] O. M. Faltinsen, *Sea loads on ships and offshore structures*. Cambridge Cambridge University Press, 1990.

[12] U. A. Korde and J. Ringwood, *Hydrodynamic Control of Wave Energy Devices*. Cambridge University Press, 2016.

[13] J. Falnes, *Ocean waves and oscillating systems: linear interactions including wave-energy extraction*. Cambridge university press, 2002.

[14] S. Liu, L. Sun, and J. Zhu, "Influence analysis of Pelamis wave energy converter structure parameters," *World Academy of Science, Engineering and Technology, International Journal of Mathematical, Computational, Physical, Electrical and Computer Engineering*, vol. 8, no. 6, pp. 930–936, 2014.

[15] K. Ruehl, C. Michelen, S. Kanner, M. Lawson, and Y.-H. Yu, "Preliminary verification and validation of WEC-Sim, an open-source wave energy converter design tool," in *Proceedings of the 33^{rd} International Conference on Ocean, Offshore and Arctic Engineering*. San Francisco, USA: American Society of Mechanical Engineers, June 2014.

[16] A. Babarit and G. Delhommeau, "Theoretical and numerical aspects of the open source BEM solver NEMOH," in *11^{th} European Wave and Tidal Energy Conference (EWTEC2015)*, 2015.